



Article

# Morphotectonic Kinematic Indicators along the Vigan-Aggao Fault: The Western Deformation Front of the Philippine Fault Zone in Northern Luzon, the Philippines

Rolly E. Rimando <sup>1,\*</sup>  and Jeremy M. Rimando <sup>2,3</sup> 

<sup>1</sup> Philippine Institute of Volcanology and Seismology, PHIVOLCS Bldg., C.P. Garcia Avenue, U.P. Campus, Diliman, Quezon City 1101, Philippines

<sup>2</sup> Department of Earth Sciences, University of Toronto, Toronto, ON M5S 3B1, Canada; jeremy.rimando@mail.utoronto.ca

<sup>3</sup> Department of Chemical and Physical Sciences, University of Toronto Mississauga, Mississauga, ON L5L 1C6, Canada

\* Correspondence: rimandogeol@gmail.com

Received: 28 January 2020; Accepted: 20 February 2020; Published: 22 February 2020



**Abstract:** The Vigan-Aggao Fault is a 140-km-long complex active fault system consisting of multiple traces in the westernmost part of the Philippine Fault Zone (PFZ) in northern Luzon, the Philippines. In this paper, its traces, segmentation, and oblique left-lateral strike-slip motion are determined from horizontal and vertical displacements measured from over a thousand piercing points pricked from displaced spurs and streams observed from Google Earth Pro satellite images. This work marks the first instance of the extensive use of Google Earth as a tool in mapping and determining the kinematics of active faults. Complete 3D image coverage of a major thoroughgoing active fault system is freely and easily accessible on the Google Earth Pro platform. It provides a great advantage to researchers collecting morphotectonic displacement data, especially where access to aerial photos covering the entire fault system is next to impossible. This tool has not been applied in the past due to apprehensions on the positional measurement accuracy (mainly of the vertical component). The new method outlined in this paper demonstrates the applicability of this tool in the detailed mapping of active fault traces through a neotectonic analysis of fault-zone features. From the sense of motion of the active faults in northern Luzon and of the major bounding faults in central Luzon, the nature of deformation in these regions can be inferred. An understanding of the kinematics is critical in appreciating the distribution and the preferred mode of accommodation of deformation by faulting in central and northern Luzon resulting from oblique convergence of the Sunda Plate and the Philippine Sea Plate. The location, extent, segmentation patterns, and sense of motion of active faults are critical in coming up with reasonable estimates of the hazards involved and identifying areas prone to these hazards. The magnitude of earthquakes is also partly dependent on the type and nature of fault movement. With a proper evaluation of these parameters, earthquake hazards and their effects in different tectonic settings worldwide can be estimated more accurately.

**Keywords:** Vigan-Aggao Fault; neotectonics; kinematics; Philippines; northern Luzon; strike-slip faulting; Philippine Fault Zone

## 1. Introduction

The major and minor active faults in northern Luzon and adjoining areas belong to a system of faults and subduction zones that accommodates part of the deformation due to the northwestward

drift of the Philippine Sea Plate (PSP) towards the Sunda Plate (SP) (Figure 1). The foremost of these faults is the Philippine Fault Zone (PFZ), with the Vigan-Aggao Fault being located in the westernmost part of this fault system.

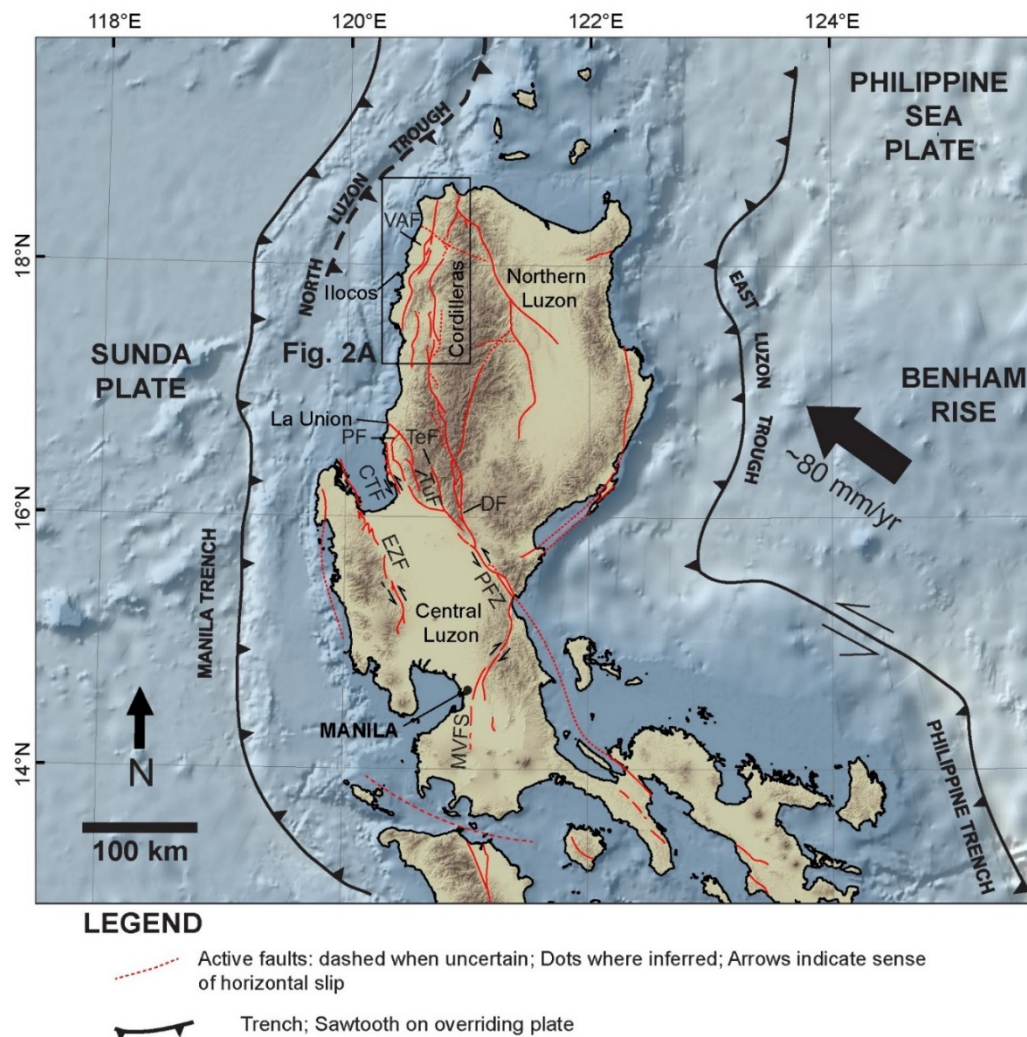


**Figure 1.** Map of known active faults in central and northern Luzon, the Philippines. CTF—Coastal Thrust Fault, PFZ—Philippine Fault Zone, VAF—Vigan-Aggao Fault, PF—Pugo Fault, TeF—Tebbo Fault, TuF—Tuba Fault, DF—Digdig Fault, EZF—East Zambales Fault, and MVFS—Marikina Valley Fault System.

How the Vigan-Aggao Fault and other major faults in the area within and in the vicinity of the PFZ accommodate crustal shortening through strike-slip and vertical slip is still uncertain, but may be clarified by a kinematic analysis of associated morphotectonic and structural features.

With the exception of a few segments of the PFZ and the Marikina Valley Fault System (or MVFS), most of the major active faults in the northern and central Luzon region have yet to be properly mapped (Figure 1).

Numerous potentially hazardous minor active faults (e.g., in central Luzon) that are located within the blocks bounded by the major active faults are not yet known, let alone mapped in detail. The lack of understanding of faulting derived from comprehensive mapping and an accurate assessment of the kinematics of structures is a source of significant uncertainty in earthquake hazard and risk assessment for the region. The recent sense of motion of some major active faults in the region, for example, may have been inaccurately labeled because the methods used for determining recent kinematics are not appropriate (e.g., the Vigan-Aggao Fault and Coastal Thrust Fault (CTF) were misconstrued

as thrust instead of strike-slip; the Bangui fault was mislabeled as strike-slip instead of normal; and the East Zambales Fault (EZF) was misconstrued as thrust instead of strike-slip). With inaccurate mapping and faulting mechanisms, the magnitude of resulting hazards and the severity of damage from earthquakes may have been greatly miscalculated. Due to our limited knowledge on these active faults, our understanding of deformation of the region resulting from plate motion is also limited. This study, in part, aims to address not only the issue on the kinematics of the Vigan-Aggao Fault, but also its continuity. In addition to its tectonic significance, a better understanding of the continuity and kinematics of the Vigan-Aggao Fault has implications for the estimation of seismic hazards it poses for nearby coastal towns of northern Luzon.

The neotectonic data generated would be useful in elucidating the deformation mechanisms of structures and the kinematic relationship of major and minor faults (e.g., MVFS, EZF, and PFZ) in two adjacent deformation environments (i.e., central and northern Luzon). This would also lead to an understanding of the plate kinematics and geometry of subducting plates and their boundaries, as well as the style, nature, and distribution in space and time of some of the deformation resulting from plate interactions in the Philippines, and their role in the overall mountain building processes.

## 2. Regional Geology and Tectonics

The PFZ accommodates (Figure 1) much of the relative movement of the two plates between the trench systems and may decouple the northwestward movement of the PSP from the southeastward movement of the Sunda plate [1,2]. Another view is that the PFZ accommodates the boundary-parallel component of the overall plate convergence as a trench-linked strike-slip fault related to the Manila trench and/or the Philippine trench [3–5]. To a certain degree, the known and predicted slips of the PFZ and most of its splays are consistent with this west-northwest to northwest motion of the PSP. The mountain range of the Cordilleras is cut by the PFZ and its branches. Among the more prominent faults in the area are the Digdig, Tebbo, Pugo, Tuba, and Coastal “Thrust” Fault [6] (Figure 1). The Cordilleras, which is composed of granodioritic bodies, shallow- to deep-sea sedimentary units, and volcanics, began uplifting during the Miocene. During the Pleistocene, the rate of its uplift is believed to have been 1.5 mm/yr [7]. About 2 cm/yr of crustal shortening is co-seismically accommodated by the Philippine fault.

The Vigan-Aggao Fault (Figure 2A) is the westernmost strand of the PFZ in northern Luzon. It represents the active deformation front along the western side of northern Luzon [7]. The strike-slip activity of the PFZ has apparently propagated westward from the Middle Miocene to the present and the Vigan-Aggao Fault has represented the active deformation front in the region since it became active in the Pliocene [8]. The folded area associated with the fault is 5 km wide [8]. Along with the left-lateral strike-slip Abra River Fault to the east, it controls the formation of the Solsona Basin based on the elevation and observed deformation of sediments adjacent to the fault.

## 3. Methodology

Many landforms suggest youthfulness and are very useful in identifying the active traces or strands of fault zones. Some authors [9–13] have related the freshness of appearance and type of geomorphic expression of faults to the age of faulting. Among the most distinctive characteristics of active strike-slip faults is an array of distinctive physiographic features [14]. Many of the features can be explained by extension or contraction through simple shear [15,16] or through their location in releasing or constraining bends or steps of fault traces [17,18]. A variety of fault-formed structures, such as pressure ridges, sag ponds, shutter ridges, and systematically offset/deflected streams, have been documented by investigators, e.g., [19–31]. Neotectonic strip maps such as those for the San Andreas Fault [32–35] and for other faults elsewhere typically show these characteristic landforms. Slemmons (1982) [11] compiled a list of the main geomorphic features which are associated with active strike-slip, thrust, and normal faults, and showed how the sense of motion deduced from the offset of these features can vary along different types of fault.

For the Vigan-Aggao Fault, the mapping of active trace and sense of motion of segments are inferred from offset values taken from each reference feature, primarily from offset spurs, which are more abundant along the whole stretch of the fault. Offset streams are as abundant, but piercing points on these provide far less reliable values for vertical separations than for horizontal offsets compared to offset spurs. We used satellite images from Google Earth for the rapid visualization, identification, and measurement of horizontal and vertical offsets from piercing points of offset reference features. The mosaic of images in Google Earth can be relied upon for horizontal offsets, but vertical separations were extracted both from these images and from ASTER (Advanced Spaceborne Thermal Emission and Reflection Radiometer) Global DEM (Digital Elevation Model) Version 2 (GDEM V2; 2011). ASTER has a more complete coverage for the study area compared to SRTM and, therefore, provides more homogeneous positional data. Google Earth and ASTER DEM are free and readily accessible. Since the results are comparable, only the results from Google Earth are presented herein.

The superimposition of digitized traces of active faults on Google Earth is becoming a standard practice for visualizing active faults, but the use of Google Earth in mapping active faults is still uncommon. This work marks the first instance of the extensive use of Google Earth as a tool in mapping and determining the kinematics of active faults. Google Earth superimposes satellite images and/or aerial photographs over DEMs. It uses DEM data from NASA's SRTM mission for its 3D capability. Although the use of Google Earth in visualizing and extracting topographic data for various applications has been increasing since it was first introduced in 2005, issues regarding the positional accuracy have perhaps limited its use to mainly visualization and display. Assessments of Google Earth's positional accuracy and applicability have provided variable results [36–39]. Surprisingly, a comparison of the accuracy of elevation data from Google Earth with those from other sources has shown that, in most places, only a limited number of sources (e.g., total station surveys, differential global positioning surveys (DGPS), or topographic maps from high-resolution aerial photography) can rival Google Earth's accuracy, which is found to be more accurate than most aerial photography-based topographic maps and, occasionally, SRTM. This is made possible by updating Google Earth with better resolution images and by its use of other technologies and alternative data sources [37]. In this study, resolution issues involved in vertical separation measurements using Google Earth and other sources of uncertainty in evaluating the sense(s) of motion are considered. Whether the uncertainty is large enough to render inferred sense(s) of motion unreliable will be a primary consideration in appreciation of the results for the Vigan-Aggao Fault area.

#### 4. Previous Studies

Earlier studies are unclear about the recent kinematics of the Vigan-Aggao Fault, e.g., [7,8,40]. In particular, detailed evidence on continuity, and the variation and controls of horizontal and vertical components of displacement, has yet to be presented [7,8,40]. The Vigan-Aggao Fault has also been linked to the Coastal Thrust Fault (CTF) in La Union as its northern extension, partly on the basis of its similarity in terms of kinematics (i.e., having a thrust component) and partly on the basis of an interpretation of offshore seismic profiles south of Vigan [41].

There remains uncertainty as to whether the Vigan-Aggao Fault has a dominantly thrust, e.g., [40,42] or strike-slip [7,8] faulting mechanism (Figure 2B). The Vigan-Aggao Fault has previously been described as an NNE- to NS-trending, east-dipping thrust fault ( $40^\circ$  to  $55^\circ$  E), with a length of 132 km from Vigan (Ilocos Sur) to Bacsil (Ilocos Norte), based on aerial photograph interpretation and observed structures [40]. Additionally, the fault between Vigan and Aggao has been characterized in terms of the range front linearity, landform "disruption", and changes in lithology, using Defense Mapping Agency (DMA) aerial photographs and synthetic aperture radar (SAR) images [40]. In contrast, the Vigan-Aggao Fault has been described as a sinistral strike-slip fault with a thrust component, based on field structural observations and an analysis of fault plane slickenlines from outcrops, and is considered the westernmost strand of the PFZ in northern Luzon [7,8]. Ringenbach (1993) [7] posited a northward increase in the thrust component of the strike-slip fault, which is consistent with Pinet and

Stephan’s (1990) [8] observations of thrust features. The fault also forms the western boundary of the Solsona basin, which is bounded by the Abra River Fault to the east. Pinet and Stephan (1990) [8] and Ringenbach (1993) [7] inferred that Plio-Quaternary convergent wrench faulting that formed a positive flower structure (of the Vigan-Aggao Fault) with a narrow, elongated ridge expression along the fault’s trace, was instrumental in the basin’s formation. The “flower structure” supposedly consists of parallel upthrusts with opposite dips and *en echelon* folding. However, no details similar to the aforementioned descriptions were provided for the segments north and south of the fault segment in the Laoag area.

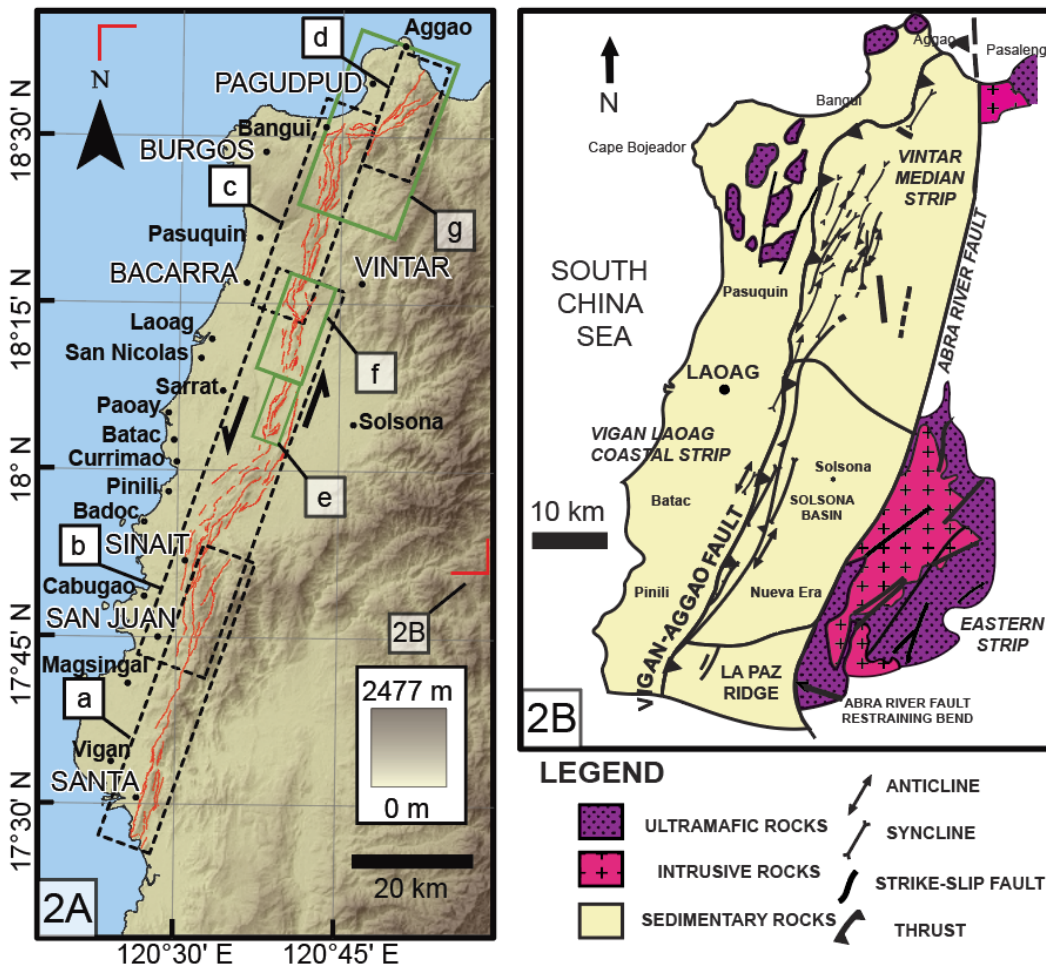


**Figure 2.** (A). Map showing a trace of the Vigan-Aggao Fault (red line), its segmentation (black dashed-line boxes; see Results and Analysis below for the segmentation criteria used), and several featured fault steps/bends (green boxes). a—Santa-Sinait segment, b—San Juan-Vintar segment, c—Bacarra-Burgos segment, d—Pagudpud segment, e—Batac-Laoag bend, f—Sarrat-Vintar-Bacarra bend, and g—Bangui-Pagudpud bend. Location indicated by the black rectangle in Figure 1B. Place names in all caps indicate the bases of fault segment names. (B). The known geology and previously assumed structure in the vicinity of the Vigan-Aggao Fault (location indicated by red corners in Figure 2A). Directly east of the Vigan-Aggao Fault is another splay of the PFZ—the Abra River Fault. To the west of the Vigan-Aggao Fault is the Vigan-Laoag Coastal Strip, which is characterized by a metamorphosed Cretaceous ultramafic basement that is uncorformably overlain by a thin Eocene to Miocene sedimentary cover. To its north are Oligocene to Early Miocene granitic bodies, which intrude the metamorphic rocks. To the east of the fault is a thick sequence of predominantly clastic sedimentary units that are as old as Late Eocene (modified after Pinet and Stephan, 1990 [8]).

A detailed analysis of displacement data from the measurement of offset morphotectonic features can allow a comprehensive and systematic clarification of the kinematics of the Vigan-Aggao Fault.

Aside from determining the fault's kinematics, our analysis also aims to address the question of the Vigan-Aggao Fault's segmentation and continuity to the south of Vigan. The Vigan-Aggao Fault is thought to be linked to the Coastal Thrust Fault in La Union, partly on the basis of the supposed similarity in the sense of slip (i.e., both are believed to be thrust faults) [2], and partly on the continuity inferred from offshore seismic profiles south of Vigan [43]. Such previous studies, however, are uncertain about the fault's northern terminus.

## 5. Results and Analysis

Numerous offset landforms and streams that indicate not only the recency of activity, but also the nature and sense of faulting, were mapped and used to delineate the active traces of the Vigan-Aggao Fault from Santa (Ilocos Sur) in the south to Pagudpud (Ilocos Norte) in the north (Figure 2A, Table S1, and Figures S1–S11). Segmentation was assessed in terms of structural, geological, and geometric criteria, as defined by Knuepfer (1989) [44] and DePolo et al. (1991) [45]. The branching of faults and intersections with other faults, changes in the fault orientation, step overs, and gaps were the primary criteria used in differentiating the segments. Based on these, three major geometric segments along the Vigan-Aggao Fault were identified, namely, the Santa-Sinait (49 km) ('a' in Figure 2A), San Juan-Vintar (65 km) ('b' in Figure 2A), and Bacarra-Burgos (31 km) ('c' in Figure 2A). A minor segment—Pagudpud (17 km) ('d' in Figure 2A)—a much shorter segment located to the north of these three major segments, was also identified.

### 5.1. Santa-Sinait Segment

The trace in the Santa-Vigan area along the Santa-Sinait segment ('a' in Figures 2A and 3) has one of the most abundant associated morphotectonic features. There are far more numerous places along the Santa-Sinait segment that show very large lateral components of left-lateral displacement (Figure 3). In some places, the vertical component of slip is conspicuously large, which might have prompted previous workers and investigators to interpret it as a thrust fault. The vertical-to-horizontal displacement (V/H) ratio for most of the Santa-Sinait area is below 1. Given the uncertainties in the estimation of the vertical component of slip, some of these could very well be assigned a V/H ratio of more than 1 (between 0 and 25 km in Figure 3). However, the majority of points correspond to less than a 0.5 V/H ratio. Unusually high V/H ratios in the Cabugao-Sinait area (left part of the graph in Figure 3) are within and proximal to an area of transtension between two left-stepping segments. It should also be noted that the sense of displacement is consistently left-lateral throughout the Santa-Sinait stretch.

Numerous examples of associated morphotectonic features (highly linear valley, saddle, triangular facets, linear ridges) and offset spurs and streams that indicate left-lateral strike-slip faulting abound along the segment (e.g., Figure 4, Figure 5, and Figure S1). The vertical component of slip is relatively large in some parts, but the larger component of left-lateral-slip does not warrant identifying this stretch as a thrust fault.

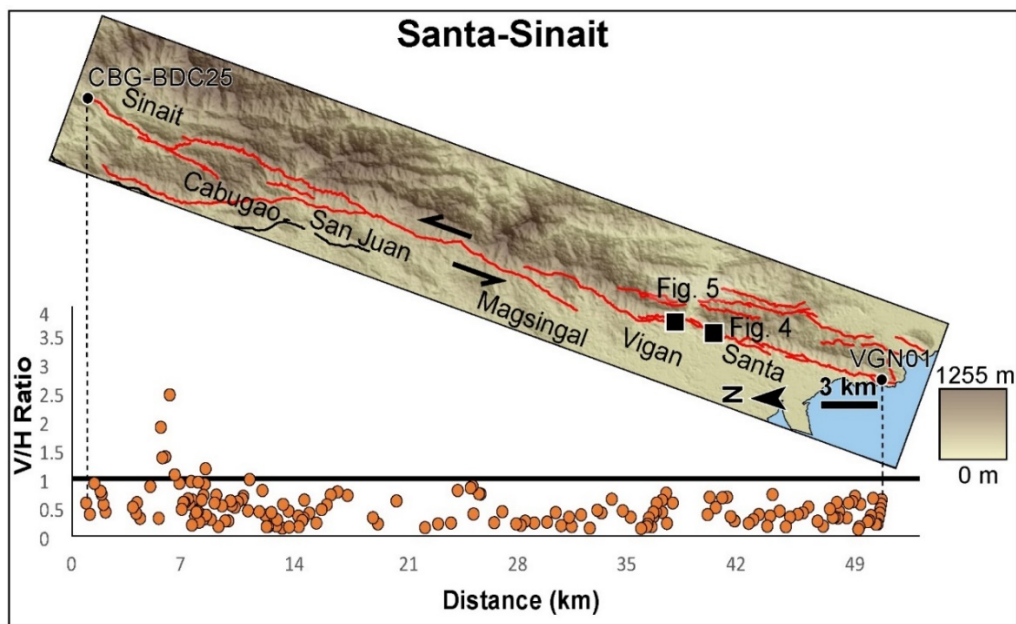


**Figure 3.** Map of the trace from Santa to Sinait (labeled ‘a’ in Figure 2A), south of Magsingal above the offset plot for this part of the Vigan-Aggao Fault. The Santa-Sinait segment is traced in red, while the southern portion of the San-Juan Vintar segment is traced in black.



**Figure 4.** Left-laterally offset spurs and stream in Santa, Ilocos, Sur. Sinistral strike-slip faulting is indicated by the dominant lateral component of slip relative to the vertical component. Location of the photo is indicated by a black square in Figure 3.



**Figure 5.** A series of left-laterally offset spurs in Vigan, Ilocos, Sur. Triangular facets are also prominent features. Location of the photo is indicated by a black square in Figure 3.

### 5.2. San Juan-Vintar Segment

The transition from the Santa-Sinait segment to the San Juan-Vintar segment ('b' in Figures 2A and 6) is marked by a break in the continuity of the Vigan-Aggao Fault. The San Juan-Vintar segment branches from the Santa-Sinait segment near San Juan, while the Santa-Sinait segment terminates east of the Sinait-Badoc area.

In the area between San Juan and Vintar (Figure 6), numerous associated morphotectonic features were also key in mapping the active traces (Figure 7, Figure 8, Figures S2, and S3). The kinematics shown by morphotectonic features along the San Juan-Vintar segment east of Sinait, Ilocos, Sur, is consistent with a left-lateral strike-slip fault. From where it branches in the San Juan area (Figure 6), the active fault can be traced relatively uninterrupted towards the north, except for minor bends and steps. In the vicinity of Badoc, however, the fault zone makes a major northeastward bend, and then returns to its essentially NNE trend in the Currimao-Paoay area (Figure 6). Along the strands of this NE bend from Sinait to Paoay (21 to 38 kms) are numerous offset features having V/H values of >1. North of this bend until the 14 km mark east of San Nicolas, elevated V/H values are associated with smaller bends ('e' in Figures 2A and 9).

From the Batac area, the trace snakes northward through smooth bends and minor steps until the east of Vintar. In the San Nicolas-Laoag area, we noted a consistency in kinematics with those displayed along the Vigan-Aggao Fault's traces south of Badoc (Figure S2). The offset and deflection of streams and spurs consistently indicate mainly left-lateral strike-slip faulting. Movement is mostly oblique, except in a few places, where the motion is almost purely left-lateral. V/H values >1 occur exclusively along major and minor bends. The variation of V/H values along the San Juan-Vintar segment reaffirm Vigan-Aggao Fault's oblique sinistral strike-slip, rather than thrust, nature.



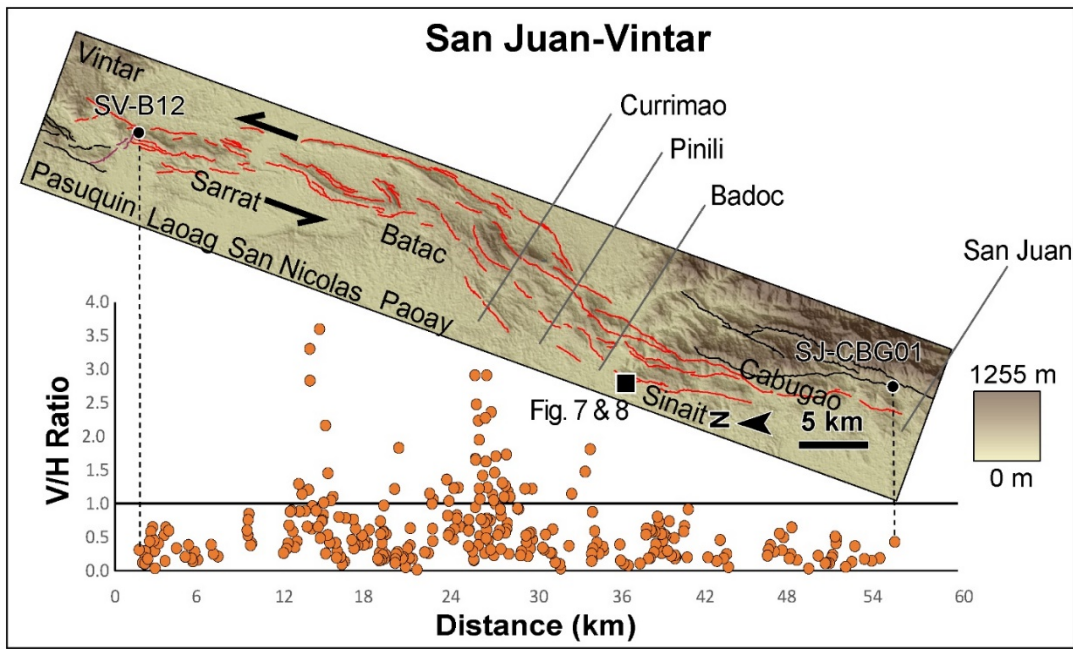


**Figure 6.** Map of the trace from San Juan to Vintar (labeled ‘b’ in Figure 2A) above the offset plot for this part of the Vigan-Aggao Fault. The fault zone is marked by a broad bend within a right-step gap. The San-Juan Vintar segment is traced in red, while the northern portion of the Santa-Sinait segment is traced in black. The transition between these segments is traced in violet.



**Figure 7.** A series of left-laterally offset spurs mark the location of the Vigan-Aggao Fault’s active trace along the highly linear mountain front in the Badoc-Sinait area (Ilocos Sur). Location of the photo is indicated by a black square in Figure 6.

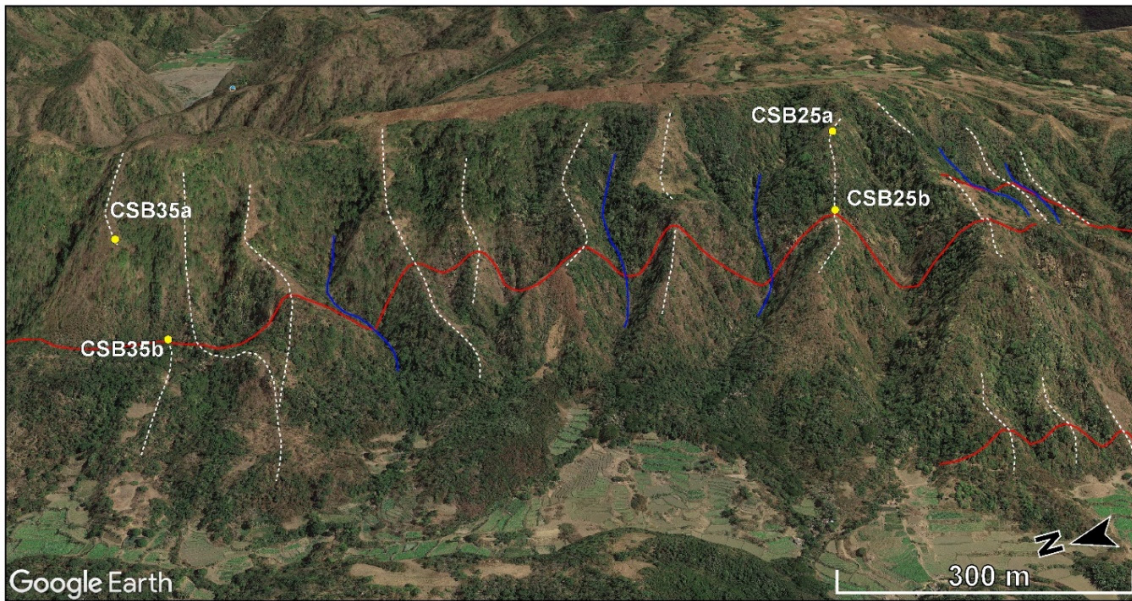


**Figure 8.** Google Earth perspective view of offset features along a stretch of the Vigan-Aggao Fault in the Badoc-Sinait area. This part of the fault is dominated by a horizontal component of slip. Location of this Google Earth perspective view is indicated by a black square in Figure 6.

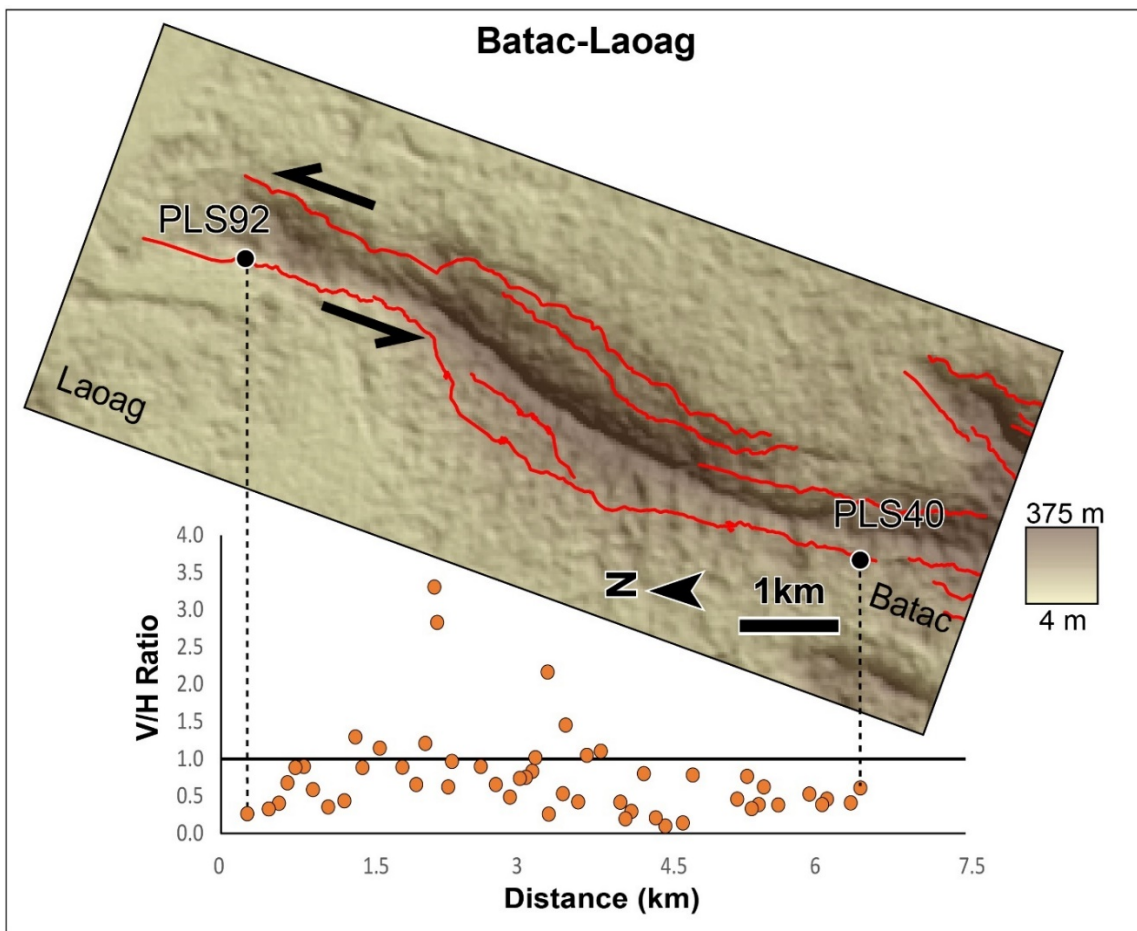


**Figure 9.** Map of the trace from Batac to Laoag (labeled ‘e’ in Figure 2A) above the offset plot for this part of the Vigan-Aggao Fault. The fault zone is also marked, at a smaller scale, by a bend within a right-step gap.

### 5.3. Bacarra-Burgos Segment

The San Juan-Vintar segment becomes discontinuous east of Vintar. An abrupt left-step marks the extension of the active fault zone farther north—the Bacarra-Burgos segment ('c' in Figures 2A and 10). The transition between the San Juan-Vintar and Bacarra-Burgos segments is marked by NW-oriented faults characterized by offset features having high V/H ratios (Figure 10). The tail ends of both the San Juan-Vintar and Bacarra-Burgos segments, on the other hand, are characterized by offset features having V/H ratios which are mostly well below 1 (Figures 10 and 11). Relatively high V/H values near the southern tail end of the Bacarra-Burgos segment are due to the influence of the localized extension within the left-step gap. The NW-oriented normal faults (Figure 11) developed due to localized extension within the gap between the left-stepping sinistral strike-slip faults. The extensional nature of the fault within this zone is supported by the mapping of both dextral and sinistral horizontal components of displacement along the normal fault (Figure 12, Figures S6, and S7).

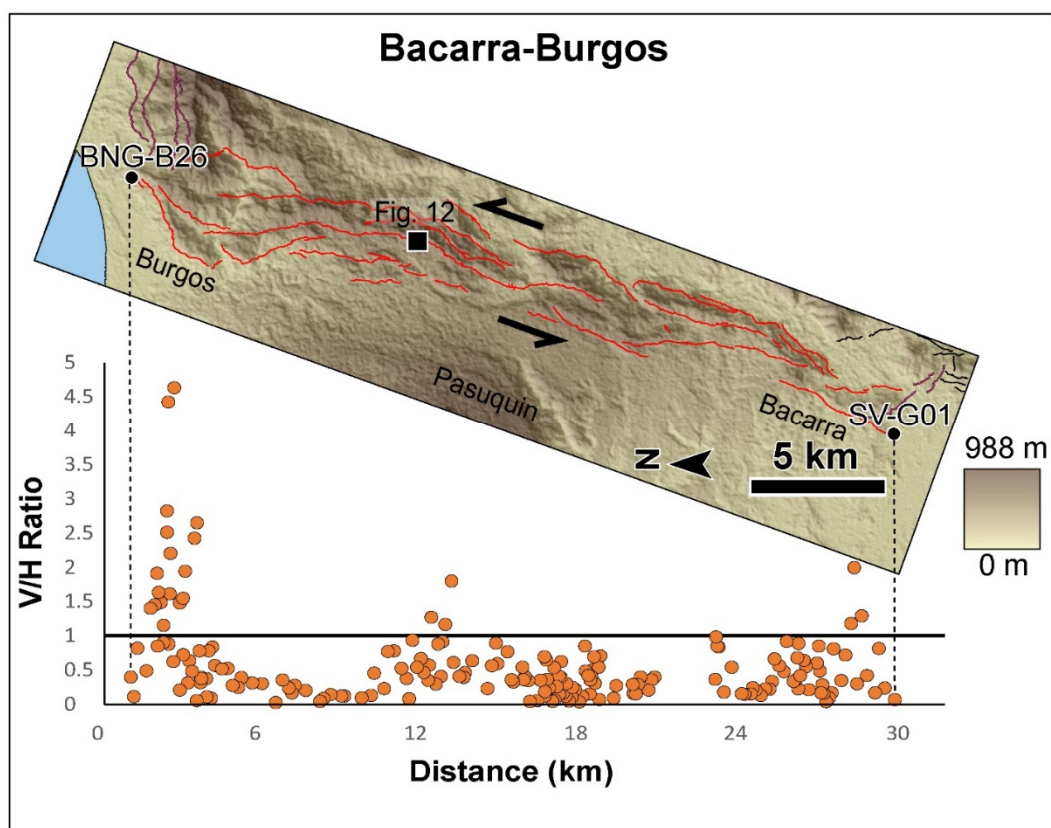


**Figure 10.** Map of the trace from Bacarra to Burgos (labeled 'c' in Figure 2A) above the offset plot for this part of the Vigan-Aggao Fault. The Bacarra-Burgos segment is traced in red, while the northern portion of the Serrat-Vintar-Bacarra segment is traced in black. The transition between segments is traced in violet.

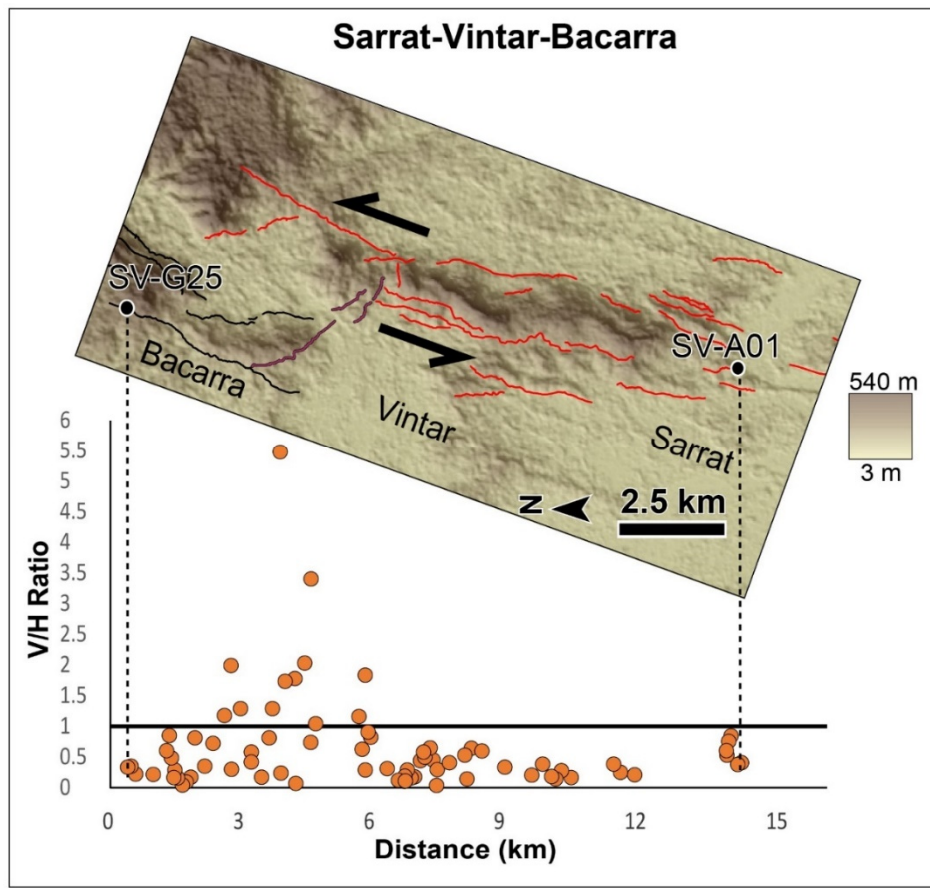


**Figure 11.** Map of the trace from Serrat to Bacarra (labeled ‘f’ in Figure 2A) above the offset plot for this part of the Vigan-Aggao Fault. The fault zone is also marked, at a smaller scale, by a bend within a left-step gap. Higher V/H values correspond to the gap between the left-stepping segments. The Serrat-Vintar-Bacarra segment is traced in red, while the southern portion of the Bacarra-Burgos segment is traced in black. The transition between these segments is traced in violet.

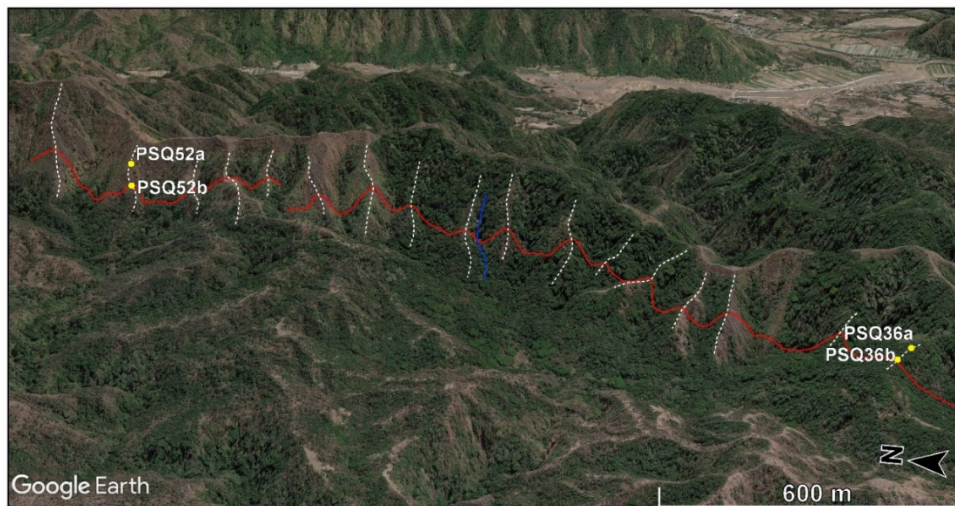


**Figure 12.** Google Earth perspective view of the middle portion of the Bacarra-Burgos segment (from 13 to 15 km, east of the Pasuquin-Burgos area) displaying elevated V/H values, which belongs to the part of the fault zone where it bends from a NE to NNE orientation. Both sinistrally and dextrally offset spurs are observed along this stretch. Location of this Google Earth perspective view is indicated by a black square in Figure 10.

The V/H values for most of the length of the Bacarra-Burgos segment are well below 1. Exceptions to this are the cluster of points with  $>1$  V/H values near the middle portion of the segment (from 13 to 15 km, east of the Pasuquin-Burgos area) and near the southern and northern tail ends of the segment. The elevated V/H values east of the Pasuquin-Burgos area belong to the part of the fault zone where it bends from a NE to NNE orientation (Figure 10). As discussed earlier, the southern tail end of the Bacarra-Burgos segment is influenced by localized extension within the left-step gap between the San Juan-Vintar segment and the Bacarra-Burgos segment. The points with high V/H ratios at the northern tail end of the Bacarra-Burgos segment fall where the N-S stretch of the segment bends northwestward. It is also influenced by localized transpression within the right-step gap between the Bacarra-Burgos segment and the northernmost segment of the Vigan-Aggao Fault—the Pagudpud segment.

#### 5.4. Pagudpud Segment

The Vigan-Aggao Fault is continuous up to the Bangui and Pagudpud area in Ilocos Norte ('g' in Figures 2A and 13) From a more northerly orientation in Pasuquin, the active trace swings towards the northeast towards Bangui, but regains its northerly trend in the Pagudpud area (Figure 13). Numerous morphotectonic features were mapped in the field along the highly linear fronts in Bangui and Pagudpud (Figures S8, S9, S10, and S11).

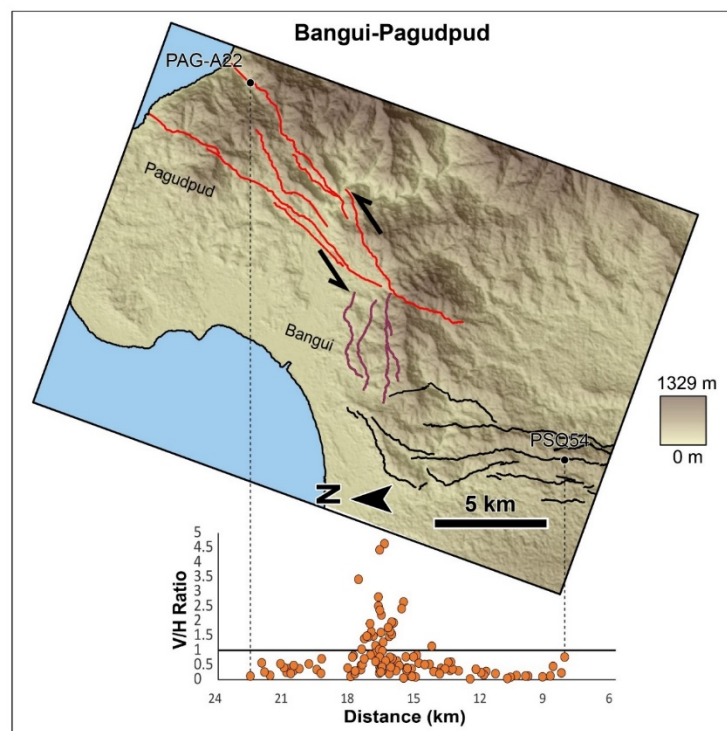


**Figure 13.** Map of the trace from south of Bangui to Pagudpud (labelled 'g' in Figure 2A) above the offset plot for this part of the Vigan-Aggao Fault. The fault zone is also marked by bends and right-step gaps. The Pagudpud segment is traced in red, while the northern portion of the Bacarra-Burgos segment is traced in black. The transition between segments is traced in violet.

In Bangui (between 15 to 18 km; Figure 13), the vertical component of slip becomes larger, partly due to the change in orientation, wherein the northern tail end of the Bacarra-Burgos segment bends from a more northerly to a more northeasterly orientation (Figures 10 and 13). The cluster of very high V/H ratios also includes those along faults within the narrow zone sandwiched by the Bacarra-Burgos and Pagudpud segments (Figures 10 and 13). As discussed earlier in this section, bends and jogs of strike-slip faults usually display large components of vertical displacement. Within the right-step gap between the Bacarra-Burgos and Pagudpud segments, those with high V/H ratios

are thrust faults (Figures 10 and 13), which developed due to localized compression within the zone. Along the Pagudpud segment, however, strike-slip fault features prevail (Figures S8, S9, S10, and S11), where almost all V/H ratios are  $<1$  and H/V values are as large as 5:1 (Figure 13). V/H values close to 1 at the southern end of the Pagudpud segment developed due to the influence of local compression in the gap area between the two segments.

## 6. Discussion and Interpretation

The Vigan-Aggao Fault is clearly a strike-slip fault rather than a thrust fault or normal fault, as suggested by earlier studies [40,42]. This is based on the associated morphotectonic features that characterize strike-slip faults and on the more dominant horizontal component of slip. Along most of the stretch of the Vigan-Aggao Fault's segments, the horizontal component of slip is much larger, as indicated by the V/H values, which were mostly below 1. The majority of the points below the  $V/H = 1$  line are lower than 0.5. Locally, a large vertical component of displacement is associated with thrust or normal faults. The locations of these zones are strongly correlated with the locations of bends and jogs. Within these regions, both dextral and sinistral sense of the horizontal component of displacement coexist. This is not the case, however, outside of these zones of bends and jogs. The segments of the Vigan-Aggao Fault outside of the jogs and bends host V/H values below 1.

The reliability of the V/H ratio as an indicator of the sense of faulting depends on how well the vertical separation (V) measurements represent the dip-slip component of displacement. The use of SRTM elevation values from Google Earth is a source of uncertainty. The use of Google Earth poses positional errors, which are greater for elevation. The degree of underestimation of elevation due to the use of SRTM values becomes greater for higher elevation areas. Moreover, the higher the piercing points and the higher the elevation difference between two piercing points, the higher the error will be. Several studies, however, have demonstrated the reliability of elevation measurements from Google Earth relative to other available tools [36–39]. Additionally, the vertical separation value may underestimate the dip-slip component of displacement, wherein the underestimation is greater for more gentle dips. The dip of the Vigan-Aggao Fault is said to be variable along its trace [46]. Because fault dips are variable, using an assumed uniform dip to estimate dip-slip introduces another source of error. The amount of underestimation from using vertical separation may not be as critical for parts of the fault with steep dips. Lastly, an underestimation/overestimation of vertical separation may also come from the varying amounts of erosion at the upthrown side and deposition of slope material on the downthrown side.

While a great majority of V/H values outside of the bends and jogs fall well below 1, borderline V/H values raise a question regarding the degree to which the dip-slip components of displacement were underestimated, considering the sources of uncertainty involved in estimating vertical displacements. However, the sense of left-lateral strike-slip are consistently sinistral outside of the jogs and bends. This reinforces the assessment that the Vigan-Aggao Fault is primarily an oblique sinistral strike-slip fault, rather than a thrust fault. This implies that the contributions of the sources of errors to the vertical separation estimates are not significant, at least in the case of the Vigan-Aggao Fault.

Oblique sinistral strike-slip faulting along the Vigan-Aggao Fault is kinematically congruent with the known sense of motion of the PFZ and its strands in northern Luzon (e.g., Tuba, Tebbo, Mirador, Abra River, Pugo, San Manuel, San Jose, Digdig, and Hapap). This is also consistent with the sense of motion of the Coastal "Thrust" Fault (CTF). The Coastal Thrust Fault (CTF) forms the northeastern boundary of the central Luzon basin (Figure 1). Only regional maps of active faults in coastal La Union are available, and these indicate a thrust mechanism of faulting for the CTF. Our own analysis, however, clearly indicates left-lateral strike-slip with a more minor vertical component of slip. This suggests that the Vigan-Aggao Fault and the CTF are, more likely, part of the PFZ in northern Luzon—a system of faults that accommodates shortening in the region, mainly through strike-slip. Left-lateral strike-slip faulting along the PFZ is consistent with this westward en masse drift of the PSP. The kinematics of the major faults in northern Luzon and northern Luzon (e.g., Bornay, Asin, Bangui Fault, and East

Zamabales Fault), which were previously indicated as either thrust or normal [6,8,40,42,43], should be verified. This should also put into proper perspective how deformation is accommodated and distributed along the major structures and geological features.

Studies on the kinematics of active faults in the northern Luzon region should help clarify deformation in the region. Such studies, however, should be detailed enough to show relative contributions and along-length variations in vertical and horizontal displacements. A detailed morphotectonic analysis for the kinematics of active faults in northern Luzon needs to be conducted to help clarify this. Maletierre (1989) [43] highlighted the contribution of significant vertical displacements along the PFZ to the uplift of the Central Cordillera due to oblique convergence between the SP and the PSP. Maletierre (1989) [43] cited the significant thrust component along the Vigan-Aggao Fault. Until this study, it is clear that details on the contribution of the vertical component of motion of the Vigan-Aggao Fault have remained largely unknown. The Abra River Fault has also been characterized as having pure strike-slip motion [6]. However, morphotectonic observations and investigations on the displacement variations along the Digdig Fault, before and after the 1990 Luzon earthquake, centered along the fault [47,48], strongly suggest that this may not be the case.

Through a detailed morphotectonic analysis comes the opportunity to assess the sense of slip of other active faults more accurately. The MVFS (Figure 1), for one, has been found to have a dominantly dextral strike-slip motion from geomorphic evidence gathered along the entire length and its segments [6,49]. Considering its right-lateral strike-slip motion, lateral extrusion of the block bounded by the PFZ and MVFS [6,49] and block rotation (both regional and local) as a complementary mechanism have been used to explain the kinematics of the MVFS [6,49].

No detailed basis and clear evidence for the kinematics of other active faults outside of the PFZ have been made available. A careful analysis of the displacement of morphotectonic features shows a dominant sense of slip different from mechanisms earlier indicated for the recent movement of some of these faults (e.g., East Zambales Fault and Bangui Fault). With a more accurate determination of the kinematics of active structures, it is easier to see how these faults fit in the overall scheme of deformation in northern Luzon as a result of the northwestward motion of the PSP.

We also estimated possible associated earthquake magnitudes for the Vigan-Aggao Fault using an equation relating the magnitude to the surface rupture length [50]. However, to assess the seismic potential of the Vigan-Aggao Fault, we must make assumptions as to whether the entire trace or only individual segments could rupture co-seismically. Due to the absence of independent paleoseismic data along this fault to support either scenario, we explored both scenarios to arrive at a seismic hazard assessment of the fault.

Assuming co-seismic rupture of individual segments, the Santa-Sinait (49 km), San Juan-Vintar (65 km), Bacarra-Burgos (31 km), and Pagudpud (17 km) segments yield magnitude estimates of  $M_W$  6.9–7.3,  $M_W$  7.0–7.4,  $M_W$  6.7–7.1, and  $M_W$  6.3–6.7, respectively. On the other hand, assuming a maximum surface rupture length of 140 km for the entire length of the Vigan-Aggao Fault yields an estimate ranging from  $M_W$  7.4 to 7.8.

## 7. Summary and Conclusions

Our morphotectonic mapping of the Vigan-Aggao Fault has revealed a complex pattern of active fault traces and segmentation. It has also provided evidence, primarily from offset spur and streams, of the active fault's sense of motion. The Vigan-Aggao Fault in Ilocos Sur and Ilocos Norte is an oblique sinistral-strike-slip fault. The sinistral nature of the fault is supported by measurements of the horizontal and vertical displacements indicating that lateral displacements are dominant along the length of the fault. Extremely high V/H ratios, characteristic of thrust and normal faults, are confined to regions in the vicinity of jogs and bends. Despite the uncertainties involved in the estimation of the vertical component of displacement using vertical separation as a proxy, the majority of the V/H values outside of the bend and jog regions are below 1 while a large part of these are below 0.5. The consistency in the sense of horizontal displacement (sinistral) outside of the zones of bends and

jogs indicates that the vertical separation measurements are reliable proxies for the dip-slip component of displacement in the case of the Vigan-Aggao Fault.

The assessment of the Vigan-Aggao Fault's kinematics is consistent with the data of Pinet and Stephan (1990) [8]. However, a more detailed delineation of the active fault's traces and a determination of its segmentation and sense of motion are provided by this study through the visualization and extraction of horizontal and vertical displacement data from numerous offset morphotectonic features. This study goes farther, and into more detail, by explaining the along-strike variation of displacement by recognizing local zones of transpression and transtension that are associated with bends and step-over gaps. Applying the method outlined herein should help verify the kinematics of other mapped and unmapped active faults, not only in the Philippines, but also in various tectonic settings.

The continuity of the Vigan-Aggao Fault with the Coastal Thrust Fault, however, must be verified. The similarity in kinematics of the CTF and the Vigan-Aggao Fault indicates that these strike-slip faults are probably part of one strike-slip system (West Ilocos Fault System). Its proximity and a sense of motion that is similar to the other splays of the PFZ form a strong argument for its inclusion within the PFZ.

Based on the length of the entire fault and its segments, the sinistral strike-slip Vigan-Aggao Fault is capable of generating earthquakes ranging in magnitude from  $M_W$  6.3 to  $M_W$  7.8. An incorrect assessment of the sense of displacement of the major faults in northern and central Luzon will result not only in the overestimation or underestimation of hazards, but also in a misleading assessment of the deformation mechanism involved and of the contributions of the major structures in accommodating deformation in the region. The contribution of thrust faulting to the overall deformation budget may have previously been overestimated. A large part of shortening through faulting across central and northern Luzon is accommodated by strike-slip faulting, mainly along the PFZ. The Vigan-Aggao Fault participates in the shortening by strike-slip faulting rather than thrust faulting. The rest of the deformation due to the westward drift of the Philippine Sea Plate is accommodated by thrust faulting elsewhere (if there is any, or by the thrust component of oblique strike-slip faults), by subduction, and by regional uplift.

**Supplementary Materials:** The following are available online at <http://www.mdpi.com/2076-3263/10/2/83/s1>, Figure S1. Google Earth perspective view of offset features along a stretch of the Santa-Vigan area. The blue line indicates an example of an offset stream, white lines indicate selected offset spur crests, while the yellow line outlines an example of an offset spur; Figure S2. A left-laterally offset spur and a pressure ridge mark the location of the Vigan-Aggao fault's active trace along the mountain front in San Nicolas, Ilocos Norte; Figure S3. Google Earth perspective view of offset features along a stretch of the Vigan-Aggao fault in the Batac-Paoay area. This part of the fault marks where it bends within a broad right-step gap. Offsets are marked by elevated vertical offset values and involving both left-lateral and right lateral slip; Figure S4. Google Earth perspective view of a series of left-laterally offset spurs along the highly linear portion of the fault in the Batac-Sarrat area; Figure S5. Google Earth perspective view of offset features along a stretch of the Vigan-Aggao fault in the Batac-Sarrat area. This part of the fault marks where it bends within a right-step gap. Offsets are marked by elevated vertical offset values and involving both left-lateral and right lateral slip; Figure S6. Google Earth perspective view of a series of left-laterally offset spurs along the highly linear portion of the San Juan-Vintar segment in the Sarrat-Vintar-Bacarra area; Figure S7. Google Earth perspective view of offset features along a stretch of the Vigan-Aggao fault in the Sarrat-Vintar-Bacarra area. This part of the fault is within a left-step gap. Offsets are marked by elevated vertical offset values and involving both left-lateral and right lateral slip; Figure S8. A series of left-laterally offset spurs with large vertical components of displacement along the trace between the Bacarra-Burgos and Pagudpud segments in Bangui, Ilocos Norte; Figure S9. Offset spurs with relatively large vertical component of displacement. Both left-lateral and right-lateral senses of slip are involved within this localized zone of transpression between the Bacarra-Burgos and Pagudpud segments in Bangui, Ilocos Norte; Figure S10. Google Earth perspective view of offset features along a stretch of the Vigan-Aggao fault in the Bangui area. This part of the fault is within a major bend. Offsets are marked by elevated vertical offset values and involving both left-lateral and right lateral slip; Figure S11. Google Earth perspective view of offset features along the northernmost segment of the Vigan-Aggao fault in Pagudpud. This part of the fault is highly linear and is characterized by offset features involving left-lateral strike slip; Table S1. Piercing point types, locations, V/H measurements, and sense of displacement.



**Author Contributions:** Conceptualization, R.E.R. and J.M.R.; methodology, R.E.R. and J.M.R.; software, R.E.R. and J.M.R.; validation, R.E.R. and J.M.R.; formal analysis, R.E.R. and J.M.R.; investigation, R.E.R. and J.M.R.; resources, R.E.R. and J.M.R.; data curation, R.E.R. and J.M.R.; writing—original draft preparation, R.E.R. and J.M.R.; writing—review and editing, R.E.R. and J.M.R.; visualization, R.E.R. and J.M.R.; supervision, R.E.R.; project administration, R.E.R.; funding acquisition, R.E.R. and J.M.R. All authors have read and agreed to the published version of the manuscript.

**Funding:** This research received no external funding.

**Acknowledgments:** We gratefully acknowledge PHIVOLCS (Philippine Institute of Volcanology and Seismology) for providing logistical support for the study, and Lito Begonia, Edwin Ariola, and Benigno Santos for field assistance. We also thank the editors of Geosciences for their assistance throughout the submission of this manuscript and two anonymous reviewers for their very helpful feedback.

**Conflicts of Interest:** The authors declare no conflicts of interest.

## References

1. Acharya, H.K.; Aggarwal, Y.P. Seismicity and tectonics of the Philippine Islands. *J. Geophys. Res. Solid Earth* **1980**, *85*, 3239–3250. [[CrossRef](#)]
2. Hamilton, W.B. Tectonics of the Indonesian region. *USA Geol. Surv. Prof. Paper* **1979**, *1078*, 345.
3. Fitch, T.J. Plate convergence, transcurrent faults, and internal deformation adjacent to southeast Asia and the western Pacific. *J. Geophys. Res.* **1972**, *77*, 4432–4460. [[CrossRef](#)]
4. Karig, D.E. Accreted terranes in the northern part of the Philippine archipelago. *Tectonics* **1983**, *2*, 211–236. [[CrossRef](#)]
5. Yeats, R.S.; Sieh, K.E.; Allen, C.R. *The Geology of Earthquakes*; Oxford University Press: Oxford, UK, 1997.
6. Rimando, R.E.; Knuepfer, P.L. Neotectonics of the Marikina Valley fault system (MVFS) and tectonic framework of structures in northern and central Luzon, Philippines. *Tectonophysics* **2006**, *415*, 17–38. [[CrossRef](#)]
7. Ringenbach, J.C.; Pinet, N.; Stéphan, J.F.; Delteil, J. Structural variety and tectonic evolution of strike-slip basins related to the Philippine Fault System, northern Luzon, Philippines. *Tectonics* **1993**, *12*, 187–203. [[CrossRef](#)]
8. Pinet, N.; Stephan, J.F. The Philippine wrench fault system in the Ilocos Foothills, northwestern Luzon, Philippines. *Tectonophysics* **1990**, *183*, 207–224. [[CrossRef](#)]
9. Matsuda, T. Magnitude and recurrence interval of earthquakes from a fault. *J. Seism. Soc. Jpn* **1975**, *28*, 269–287.
10. Slemmons, D.B. *Faults and Earthquake Magnitude*; Paper S-73-1; Report 6; Waterways Experiment Station: Vicksburg, MI, USA, 1977; p. 129.
11. Slemmons, D.B. A procedure for analyzing fault-controlled lineament and active fault. In Proceedings of the 3rd International Conference on Basement Tectonics, International Basement Tectonics Association, Salt Lake City, UT, USA, 1982; Volume 33, pp. 33–49.
12. Wallace, R.E. Profiles and ages of young fault scarps, north-central Nevada. *Geol. Soc. Am. Bull.* **1977**, *88*, 1267–1281. [[CrossRef](#)]
13. Wallace, R.E. Geometry and rates of change of fault-generated range fronts, north-central Nevada. *J. Res. U. S. Geol. Surv.* **1978**, *6*, 637–650.
14. Sylvester, A.G. Strike-slip faults. *Geol. Soc. Am. Bull.* **1988**, *100*, 1666–1703. [[CrossRef](#)]
15. Sylvester, A.G.; Smith, R.R. Tectonic transpression and basement-controlled deformation in San Andreas fault zone, Salton Trough, California. *AAPG Bull.* **1976**, *60*, 2081–2102.
16. Wilcox, R.E.; Harding, T.P.; Seely, D.R. Basic wrench tectonics. *Bull. Assoc. Am. Pet. Geol.* **1973**, *57*, 74–96.
17. Crowell, J.C. Origin of Late Cenozoic basins in Southern California. *AAPG Bull.* **1973**, *57*, 774.
18. Dibblee, T.W., Jr. Strike-Slip Tectonics of the San Andreas Fault and Its Role in Cenozoic Basin Evolvement. In *Late Mesozoic and Cenozoic Sedimentation and Tectonics in California*; San Joaquin Geological Society: Bakersfield, CA, USA, 1977; pp. 26–38.
19. Burtman, V.S. Faults of middle Asia. *Am. J. Sci.* **1980**, *280*, 725–744. [[CrossRef](#)]
20. Buwalda, J.P. Shutter ridges, characteristic physiographic features of active faults. *Geol. Soc. Am. Proc.* **1937**, *1936*, 307.
21. Cotton, C.A. *Landscape*, 2nd ed.; Cambridge University Press: Cambridge, UK, 1948; 509p.

22. Kuchai, V.K.; Trifonov, V.G. A Young Left-Lateral Displacement in the Darvaz-Karakul Fault Zone. *Geotectonics* **1977**, *11*, 218–226.
23. Rand, W.W. *Preliminary Report of the Geology of Santa Cruz Island; Santa Barbara County, California*; California Division of Mines and Geology: Sacramento, CA, USA, 1931; Volume 27, pp. 214–219.
24. Ransome, F.L. The probable cause of the San Francisco earthquake. *Natl. Geogr. Mag.* **1906**, *17*, 280–296.
25. Rimando, R.E.; Punongbayan, R.S.; Tungol, N.M.; Mirabueno, H.T.; Nelson, A.R.; Personius, S.F. *Recent Activity, Kinematics and Regional Tectonic Setting of the Marikina Valley Fault System [Abstract]: GEOCON '95-VIII Annual Geological Convention Proceedings*; Geological Society of the Philippines: Mandaluyong City, Philippines, 1995; pp. 21–22.
26. Russell, R.J. Recent horizontal offsets along the Haywards fault. *J. Geol.* **1926**, *34*, 507–511. [[CrossRef](#)]
27. Sieh, K.E.; Jahns, R.H. Holocene activity of the San Andreas fault at Wallace creek, California. *Geol. Soc. Am. Bull.* **1984**, *95*, 883–896. [[CrossRef](#)]
28. Wallace, R.E. Structure of a portion of the San Andreas rift in southern California. *Geol. Soc. Am. Bull.* **1949**, *60*, 781–806. [[CrossRef](#)]
29. Wallace, R.E. Notes on stream channels offset by the San Andreas fault, southern Coast Ranges, California. In Conference on Geologic Problems of the San Andreas Fault System. *Stanf. Univ. Publ. Geol. Sci.* **1968**, *11*, 6–21.
30. Wallace, R.E. The Talas-Fergana Fault, Kirghiz and Kazakh, USSR. *Earthq. Inform. Bull. (USGS)* **1976**, *8*, 4–13.
31. Weiqi, Z.; Decheng, J.; Peizhen, Z.; Molnar, P.; Burchfield, B.C.; Qidong, D.; Fangmin, S. Displacement along the Haiyuan fault associated with the great 1920 Haiyuan, China, earthquake. *Bull. Seismol. Soc. Am.* **1987**, *77*, 117–131.
32. Clark, M.M. *Map Showing Recently Active Breaks along the San Andreas Fault and Associated Faults between Salton Sea and Whitewater River-Mission Creek*; U. S. Geological Survey: Reston, VA, USA, 1984.
33. Davis, T.; Duebendorfer, E. *Strip Map of the Western Big Bend Segment of the San Andreas Fault*; Map & Chart Series MC-60; Geological Society of America: New York, NY, USA, 1987.
34. Schubert, C. Neotectonics of a Segment of the San Andreas Fault, Southern California (USA). *Eliszeitalter u. Ggw.* **1982**, *32*, 13–22.
35. Vedder, J.G.; Wallace, R.E. Map Showing Recently Active Breaks along the San Andreas and Related Faults between Cholame Valley and Tejon Pass. Available online: <https://pubs.er.usgs.gov/publication/i574> (accessed on 21 February 2020).
36. El-Ashmawy, K.L. Investigation of the accuracy of google earth elevation data. *Artif. Satell.* **2016**, *51*, 89–97. [[CrossRef](#)]
37. Hoffmann, E.; Winde, F. Generating high-resolution digital elevation models for wetland research using Google Earth™ imagery: An example from South Africa. *Water SA* **2010**, *36*, 53–68.
38. Mohammed, N.Z.; Ghazi, A.; Mustafa, H.E. Positional accuracy testing of Google Earth. *Int. J. Multidiscip. Sci. Eng.* **2013**, *4*, 6–9.
39. Sharma, A.; Gupta, D. Derivation of topographic map from elevation data available in google earth. *Civ. Eng. Urban Plan. Int. J. (CiVEJ)* **2014**, *1*, 14–21.
40. Geomatrix Consultants. *Baguio-Bontoc-Banaue Road (Halsema Road) Pre-Design Investigations: Part III—Seismic Studies: Final Technical Report Submitted to the Department of Public Works and Highways*; Department of Public Works and Highways: Manila, Philippines, 1996.
41. Pinet, N.; Stephan, J.F. The Ilocos foothills and western Central Cordillera: A key region for the understanding of the geodynamic evolution of the eastern Eurasian margin in Luzon area (Philippines). In *Tectonics of the Circum-Pacific Continental Margins, Proceedings of the 28th International Geological Congress, July 9–19 1989, Washington, DC, USA*; Taylor & Francis: Abingdon, UK, 1990; pp. 165–180.
42. Intera. Geological radar interpretation of airborne SAR imagery for Luzon, Philippines (Scale 1: 100,000). In *Technical Report, Earthquake Reconstruction Project*; Department of Public Works and Highways: Manila, Philippines, 1995.
43. Maletterre, P. Histoire Sedimentaire, Magmatique, Tectonique et Metallogenique d'un Arc Oceanique Deforme en Regime de Transpression. Ph.D. Thesis, Universite Bretagne Occidentale, Brest, France, 1989; 304p.
44. Knuepfer, P.L.K. Implications of the characteristics of end-points of historical surface fault ruptures for the nature of fault segmentation. In *Fault Segmentation and Controls of Rupture Initiation and Termination*; Open-File Report; US Geological Survey: Reston, VA, USA, 1989; Volume 89, pp. 193–228.

45. DePolo, C.M.; Clark, D.G.; Slemmons, D.B.; Ramelli, A.R. Historical surface faulting in the Basin and Range province, western North America: Implications for fault segmentation. *J. Struct. Geol.* **1991**, *13*, 123–136. [[CrossRef](#)]
46. Nelson, A.R.; Personius, S.F.; Rimando, R.E.; Punongbayan, R.S.; Tungol, N.; Mirabueno, H.; Rasdas, A. Multiple large earthquakes in the past 1500 years on a fault in metropolitan Manila, the Philippines. *Bull. Seismol. Soc. Am.* **2000**, *90*, 73–85. [[CrossRef](#)]
47. Nakata, T.; Sangawa, A.; Hirano, S. A report on tectonic landforms along the Philippine fault zone in Northern Luzon, Philippines. *Sci. Rep. (7th Ser.-Geogr.)* **1977**, *27*, 69–93.
48. Punongbayan, R.S.; Rimando, R.E.; Daligdig, J.A.; Besana, G.M.; Daag, A.S.; Nakata, T.; Hiruyuki, T. Ground rupture of the Luzon earthquake. In *GEOCON '90—III Annual Geological Convention Proceedings, Special Session on Earthquake Geology and Earthquake Related Hazards*; Geological Society of the Philippines: Mandaluyong City, Philippines, 1991; Volume 1, pp. 13–37.
49. Rimando, R.E. Neotectonic and Paleoseismic Study of the Marikina Valley Fault System, Philippines. Ph.D. Dissertation, State University of New York at Binghamton, Binghamton, NY, USA, 2002; 232p.
50. Wells, D.L.; Coppersmith, K.J. New empirical relationships among magnitude, rupture length, rupture width, rupture area, and surface displacement. *Bull. Seismol. Soc. Am.* **1994**, *84*, 974–1002.



© 2020 by the authors. Licensee MDPI, Basel, Switzerland. This article is an open access article distributed under the terms and conditions of the Creative Commons Attribution (CC BY) license (<http://creativecommons.org/licenses/by/4.0/>).